Unsteady aerodynamics of lift regulation during a transverse gust encounter

Girguis Sedky,[1,*] Francis D. Lagor,[2,†] and Anya Jones[1,‡]
[1]*Department of Aerospace Engineering, University of Maryland, College Park, Maryland 20742, USA*
[2]*Department of Mechanical and Aerospace Engineering, University at Buffalo, The State University of New York, Buffalo, New York 14260, USA*

(Received 5 February 2020; accepted 17 June 2020; published 21 July 2020)

This paper presents an unsteady discrete vortex model to simulate the unsteady aerodynamics of a wing encountering a large-amplitude transverse gust with a sine-squared velocity profile. The model is used to investigate wing-gust encounters and the impact of closed-loop control on mitigating the gust. A simple proportional closed-loop control law based on pitching input about the wing's midchord is selected to regulate lift during a gust encounter by evaluating its rejection of lift disturbances using Theodorsen's unsteady aerodynamic model. The control law is tested on the discrete vortex model and is shown to reduce the peak lift coefficient of the gust encounter by 92.3% for gust ratio GR $= V_{\max}/U_\infty = 0.50$ and by 91.8% for GR $= 1.00$. The flow field and vorticity shedding behavior of the leading edge is studied and the effect of closed-loop control on the circulatory contribution to lift is discussed. The total lift force is decomposed into its individual contributions to study the various mechanisms involved in achieving the lift regulation objective.

DOI: 10.1103/PhysRevFluids.5.074701

I. INTRODUCTION

Air vehicles of all scales respond to large-amplitude gust encounters [1,2]. Commercial aircraft are susceptible to gusts induced by large-scale turbulent flow structures in the atmospheric boundary layer [3,4] and micro air vehicles (MAVs) are susceptible to gusts arising from unsteady flows present in air wakes, complex terrains, and urban environments [5]. Large-amplitude gusts encountered during flight cause large lift transients that can immediately damage the vehicle or induce unsteady loading that may fatigue the vehicle's structure over time [6]. The possible dire consequences of gust encounters have spurred a large number of studies to understand the unsteady aerodynamics of wing-gust encounters [7–9] and to develop active and passive means for gust alleviation [10–12].

Some passive means of regulating lift include the introduction of articulated wings [11] and vortex generators [13], which control flow behavior without any control input. Active means of regulating lift can be accomplished through the use of moving control surfaces [10], flapping wings [12], or synthetic jets [14], all of which require a control input to successfully regulate the aerodynamic loads. In this work, an active control method is pursued with the objective of regulating lift during a large-amplitude transverse gust encounter. This is implemented using a closed-loop control framework with a pitch acceleration control input. In Ref. [15] we demonstrated the successful application of proportional feedback control to mitigate the lift transient during a wing-gust encounter. In the present work, the proportional feedback gain is selected in a principled

*gsedky@umd.edu
†flagor@buffalo.edu
‡arjones@umd.edu

manner and the unsteady flow structures under closed-loop feedback control are studied. To design the closed-loop control law, the aerodynamic response of the wing to its pitch acceleration input is modeled using the classic theory of Theodorsen [16] and the effect of the gust on lift is treated as a disturbance that must be rejected. Brunton and Rowley [17] cast Theodorsen's unsteady aerodynamic model into a state-space form and constructed a robust controller that tracks a reference lift coefficient by varying pitch angle. The present work builds off of [17] by constructing a robust controller to reject gusts via active pitch control during a sine-squared gust encounter and studying the control's impact on the aerodynamic response and the flow field.

Previous works have investigated the fundamental flow physics of large-amplitude low-Reynolds-number gust encounters [18–21]. Perrotta and Jones [18] investigated the aerodynamic response of a flat plate encountering a traverse gust with a sine-squared velocity profile and observed strong leading- and trailing-edge vortex shedding behavior. The shedding led to large aerodynamic force transients that persisted even after the wing exited the gust. Badrya and Baeder [19] numerically investigated wing-gust encounters for geometric angles of attack of $\alpha = 0^\circ$ and $\alpha = 45^\circ$ and different gust widths. They observed that both the angle of attack and the gust width nonlinearly influenced the behavior of the massively separated flow over the wing and the resulting force transients. Corkery and Babinsky [20] carried out an experimental investigation to examine the various aerodynamic force contributions experienced during the encounter of a flat plate with a transverse top-hat gust. They concluded that the apparent added-mass force experienced by the wing due to the gust is not precisely a product of added mass, but is a noncirculatory force that arises due to the formation of a noncirculatory vortex sheet that is induced by the free vorticity of the gust. Andreu Angulo *et al.* [21] compared the unsteady aerodynamics between a wing encountering a transverse top-hat gust and a sine-squared gust. They found that the discrepancy between the classical linear Küssner lift response and the experimental measurements for a top-hat gust increased as the gust ratio $\mathrm{GR} = V_{\max}/U_\infty$ increased, highlighting the increase in nonlinear aerodynamic behavior for increasing gust strengths. The aforementioned studies suggest that gust encounters lead to the emergence of complex, nonlinear, and unsteady aerodynamic behaviors involving a diverse set of flow structures. It is expected that incorporating closed-loop control to maneuver the wing to mitigate gust encounters may give rise to new flow features. Consequently, the unsteady aerodynamics of gust encounters under closed-loop pitch actuation are studied here to determine how closed-loop control influences the flow behavior and regulates lift.

Low-order vortex modeling techniques have been extensively used to study the unsteady aerodynamics of wings at a low computational cost [22–24]. More recently, these unsteady discrete vortex methods have also been used to study wing-gust encounters [25–27]. Chen and Jaworski [27] simulated the aeroelastic interaction of a Joukowski wing encountering a vortex gust for different gust strengths and trajectories. Results from the discrete vortex model were found to match experiments well when the vortex gust is far from the wing. However, the computational expedience of these models came at the cost of omission of viscous flow physics from the simulations. The lack of viscous dissipation and viscous vortex-boundary-layer interaction from the discrete vortex model led to significant deviation of its results from experiments when the vortex gust was close to the wing. Some researchers have found success with discrete vortex hybrid methods and data assimilation techniques to alleviate the aforementioned problem. Darakananda *et al.* [25] assimilated surface pressure measurements obtained from high-fidelity computational fluid dynamics using an ensemble Kalman filter (EnKF) into a low-order discrete vortex model and examined the improvement in force predictions for an impulsively started flat plate with and without gust encounters. They found that the assimilation of pressure measurements using an EnKF was equivalent to applying a random-walk algorithm to the shed vortices, approximating viscous diffusion. Hou *et al.* [26] utilized a machine-learning algorithm to estimate aerodynamic quantities from the instantaneous surface pressure signal obtained using an unsteady discrete vortex model for a flat-plate gust encounter. In both of these studies, the flux of vorticity leaving the leading edge was modified as a surrogate for an incident transverse gust. This surrogate gust representation captures the impact of the gust on the development of the leading-edge vortex (LEV), but fails to

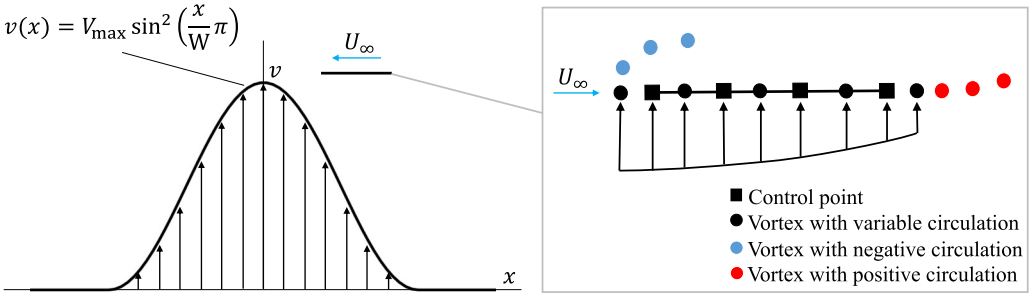

FIG. 1. Unsteady discrete vortex model components.

capture the upwash experienced by the wake from the transverse gust as well as the noncirculatory force contribution the wing experiences due to the temporal flow-field velocity gradient that the wing experiences as it travels through the gust. The success of these methods at capturing massively separated flow physics with low computational expense makes them a great candidate to test various closed- and open-loop gust mitigation strategies. The present work develops an unsteady discrete vortex method to study the aerodynamics and the unsteady flow field of a transverse wing-gust encounter under the action of closed-loop control. The transverse gust is modeled using a transverse velocity distribution that affects the wing and its wake. In future work, data assimilation and other hybrid methods may be used with the discrete vortex method presented in this work to improve force estimation.

This paper contributes the following to the understanding and modeling of gust encounters under closed-loop pitch control: (i) a low-order unsteady discrete vortex model for unsteady aerodynamic gust encounters, (ii) a closed-loop controller effective at regulating lift during a large-amplitude transverse gust encounter, and (iii) a study of the influence of lift regulation using closed-loop pitch control during a large-amplitude transverse gust encounter on the resulting flow structures and unsteady aerodynamics. These contributions offer tools for understanding how a pitch-actuated wing can interact with coherent flow structures to regulate lift.

II. UNSTEADY DISCRETE VORTEX METHOD FOR A GUST ENCOUNTER

In this section, an unsteady discrete vortex model is constructed to simulate the aerodynamic response of a two-dimensional flat plate, based on the method of Katz and Plotkin [23]. The impulse method of Wu [28] is used to evaluate the lift force experienced by the wing and the unsteady model is compared against experimental data and the well-established unsteady aerodynamic theory of Küssner [7].

A. Model construction

In the unsteady discrete vortex method of Katz and Plotkin [23], a flat plate is modeled by an infinitely thin sheet composed of a series of control points and bound vortices as shown in Fig. 1. No penetration of the plate is enforced by requiring the normal velocity at each control point to be zero. Trailing-edge vorticity shedding is modeled by enforcing the Kutta condition at the trailing edge. Modeling leading-edge shedding is less straightforward, and there are a variety of methods to do so. Two of the most popular methods for modeling leading-edge shedding are enforcing the Kutta condition at the leading edge [29,30], and modulating the vorticity shed from the leading edge using an empirically determined leading-edge suction parameter [24,31]. In this work, the enforcement of the Kutta condition is chosen to determine the vorticity shed at the leading edge. This decision is based on previous work by Manar and Jones [29] where the validity of enforcing the Kutta condition at the leading edge of a flat plate was investigated by comparing the circulation of

the leading-edge vortex for a discrete vortex model to results from experiments. In the present work, the Kutta condition is implicitly enforced at the edges of the plate due to the presence of control points there. A unique solution for the bound vortex sheet is determined by enforcing Kelvin's circulation theorem, ensuring that the total circulation in the domain always sums to zero.

For each vortex element, a Lamb-Oseen vortex core of a constant radius r_c and induced velocity

$$v_\theta = \frac{\Gamma}{2\pi r}\left(1 - e^{-r^2/r_c^2}\right) \tag{1}$$

is used to avoid nonphysically large velocities close to the vortex center. At each time step, two vortices of to-be-determined strengths are placed in the vicinity of the leading and trailing edges. These vortex elements represent the newly shed vorticity from the edges of the plate. The induced velocity normal to each control point due to the plate's kinematics as well as the free vorticity in the flow is found, and subsequently the strengths of the bound vortices and newly shed vortices are found subject to Kelvin's circulation theorem. The wake and the newly shed vortex elements are then allowed to advect with the surrounding flow field.

Figure 1 shows a sketch of a two-dimensional flat plate encountering a sine-squared transverse gust. The profile of vertical velocity at horizontal location x for a sine-squared gust with gust width W and a maximum transverse velocity $V_{\max}$ is

$$v(x) = V_{\max} \sin^2\left(\frac{x}{W}\pi\right). \tag{2}$$

The nondimensional measure of the gust strength is the gust ratio

$$\mathrm{GR} = \frac{V_{\max}}{U_\infty}, \tag{3}$$

where U_∞ is the freestream speed. In this work, time is measured in nondimensional convective time

$$t^* = \frac{tU_\infty}{c}, \tag{4}$$

where c is the chord length of the wing. The discrete vortex model is an inviscid model with vorticity concentrated in singular discrete elements. Thus, these results are valid in aerodynamic conditions where either viscous effects (viscous dissipation) are low or during short and transient unsteady conditions where viscous dissipation has not had enough time to dissipate the flow structures, the latter of which is the case in this work. Thus, in this context, they can be relevant to the scales of large aircraft or small MAVs so long as the gust happens quick enough that the timescale of the gust encounter is much faster than the timescale of dissipation. The gusts studied have gust ratios $\mathrm{GR} = 0.50$ and 1.00, which indicates that they are of the same order of magnitude as the freestream. This is common in MAV flight [32] due to their low flight speeds and low operational altitudes well within the atmospheric boundary layer where wakes may be engendered by local surface obstructions [33]. In addition, the control pitch rates required to attenuate the gust load is achievable for a small-scale agile vehicle.

Some works [34,35] model transverse gusts using a velocity field, while others capture the effect of the gust using a discrete vortex element sheet that captures the vorticity within the gust shear layers [20,36]. Prior work [36] developed a discrete vortex sheet representation to capture a transverse sine-squared gust profile, which allows gust deformation to be modeled. However, no significant improvement in the force trends was found despite an increase in the computational time required to track the discrete vortex elements used to represent the gust. In this work, the gust is modeled as a velocity field and the transverse velocity contribution of the gust is imposed on the wing's control points, bound vortices, and shed vortices according to their positions within the gust, as shown in Fig. 1.

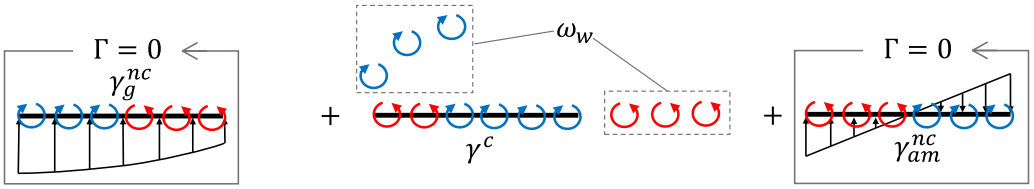

FIG. 2. Vorticity contributions for a pitching wing in a gust encounter.

B. Force evaluation using the vorticity impulse method

Unsteady forces can have numerous circulatory and noncirculatory contributions. Consequently, the forces on the wing are evaluated using the vorticity impulse method of Wu [28], which provides a comprehensive framework to evaluate the aggregate unsteady force experienced by a wing given full knowledge of the flow field's vorticity.

Consider an incompressible fluid with density ρ in a two-dimensional domain A containing vorticity $\boldsymbol{\omega}$ that is a function of position $\boldsymbol{r}$. The instantaneous vorticity impulse of this flow field is [28]

$$\boldsymbol{I} = \rho \int_A \boldsymbol{r} \times \boldsymbol{\omega}\, dA. \tag{5}$$

Since the lift force perpendicular to the freestream is of primary interest, the impulse component in the y direction

$$I_y = -\rho \int_A x\omega\, dA \tag{6}$$

is utilized. The lift force can be expressed as a function of the time derivative of the impulse of the fluid and the velocity of the body immersed in it,

$$L = -\frac{dI_y}{dt} + \rho \frac{d}{dt} \int_{A_b} v_y dA, \tag{7}$$

where A_b and v_y are the area of the immersed body and its vertical velocity components, respectively. Note that for an infinitely thin plate, the second term in Eq. (7) vanishes. Lift values are normalized using the freestream velocity to obtain the coefficient of lift

$$C_l = \frac{L}{\frac{1}{2}\rho U_\infty^2 c}. \tag{8}$$

A portion of the vorticity in the domain is bound to the plate and is called the bound vorticity, with vortex sheet strength given by γ_b. Corkery and Babinsky [20] deconstructed the bound vortex sheet strength of a plate encountering a gust into components depending on the origin of the vorticity contribution. They expressed the bound vortex sheer strength as

$$\gamma_b = \gamma_g^{nc} + \gamma^c + \gamma_{am}^{nc}, \tag{9}$$

where γ_g^{nc} is the noncirculatory contribution due to the gust, γ^c is the circulatory contribution due to the wake, and γ_{am}^{nc} is the noncirculatory contribution due to the unsteady motion of the plate.

Figure 2 illustrates the contributions to bound vorticity for a pitching wing encountering a gust. When the wing is within the gust, the gust's transverse velocity field induces a bound vortex sheet γ_g^{nc} along its chord. Since the gust has no net circulation, neither does its induced bound vortex sheet [20]. The vorticity distribution of the flow field, the gust, and the motion of the wing influence the wing's shedding behavior and the convection of the wake's vorticity ω_w. The wake in turn induces a circulatory bound vortex sheet γ^c on the wing. Since the wake has a net circulation, so does the circulatory, induced bound vortex sheet. The unsteady motion of the wing induces a noncirculatory bound vortex sheet γ_{am}^{nc}, which is the vortex sheet responsible for the added-mass force. Vortex sheet

γ_{am}^{nc} has no net circulation. During a gust encounter, the gust influences the forces experienced by the wing directly through the noncirculatory bound gust vortex sheet γ_g^{nc} and indirectly through its influence on the shed wake ω_w and the circulatory bound vortex sheet γ^c [20].

Given the contributions to the bound vortex sheet in Eq. (9) and the earlier discussion, the impulse in Eq. (6) can be decomposed into its individual contributions

$$I_y = \overbrace{-\rho \int_l x\gamma_g^{nc} dl}^{\text{I}} \overbrace{-\rho\left(\int_l x\gamma^c dl + \int_{A_f} x\omega_w dA\right)}^{\text{II}} \overbrace{-\rho \int_l x\gamma_{am}^{nc} dl}^{\text{III}}, \tag{10}$$

where A_f is the fluid domain without the plate and l is the domain of the plate. Component I is the noncirculatory gust contribution to the impulse that is a function of the rate of change of the noncirculatory bound vortex sheet induced by the gust. This contribution to the impulse gives rise to the apparent added-mass force observed during gust encounters, which differs from the classical added-mass force. Component II is the circulatory contribution of the impulse. This contribution is a function of the rate of change of the circulatory bound vortex sheet and the shed wake. The gust impacts this contribution indirectly by influencing the amount of vorticity shed from the wing's leading and trailing edges, as well as modifying the wake's motion. Component III is the contribution of the noncirculatory bound vortex sheet that is induced by the unsteady motion of the wing, which gives rise to the classical added-mass force. The decomposition of the impulse presented by Eq. (10) is useful for decomposing the total lift into its noncirculatory added-mass, noncirculatory gust, and circulatory components. This decomposition is shown later in Sec. IV.

C. Comparison with classical theory and experimental data

Two of the main classical unsteady aerodynamic models applicable to this work are Theodorsen's unsteady aerodynamic model and Küssner's sharp-edged gust model. Theodorsen's unsteady aerodynamic model gives a solution for the unsteady air loads on a two-dimensional harmonically oscillating airfoil, while Küssner's sharp-edged gust model gives a solution for the unsteady air loads on a wing encountering an infinitely wide transverse step gust [37]. These two models were both derived using potential flow analysis for incompressible inviscid flows with a planar wake and small-amplitude disturbances [37]. Even though Theodorsen's unsteady aerodynamic model was originally derived for a harmonically oscillating airfoil, it is equivalent to Wagner's indicial response in the frequency domain [17], which can be generalized to airfoils undergoing arbitrary maneuvers. Küssner's sharp-edged gust model can be generalized to transverse gusts with arbitrary shapes using a Duhamel integral [37].

The unsteady C_l time response for a flat plate with an angle of attack $\alpha = 0^\circ$ encountering a sine-squared gust is evaluated using the discrete vortex model and compared to Küssner's sharp-edged gust response with a Duhamel integral [37],

$$C_l = \frac{2\pi}{U_\infty} \int_0^{s_c} \frac{dv_{\text{LE}}(\sigma)}{ds_c} \Psi(s_c - \sigma) d\sigma, \tag{11}$$

where s_c is the distance traveled by the flat plate in semichords, v_{LE} is the transverse gust velocity experienced at the leading edge at a particular instant, and $\Psi(\cdot)$ is Küssner's function. To replicate Küssner's attached flow assumption in the discrete vortex model, the flat plate is allowed to shed vorticity only from its trailing edge. The flow during large-amplitude transverse gust encounters is known to separate at the leading edge, and thus leading-edge vorticity shedding is enforced in the discrete vortex model (DVM) for the rest of the comparisons presented in this section. Note that Eq. (11) applies at each instant in time represented by $s_c = 2t^*$, where $t^* = U_\infty t/c$ is the nondimensional convective time elapsed. To find the C_l time history, Eq. (11) is evaluated for increasing values of s_c. The gray region in the figures presented in this paper indicates the period of time during which the wing is fully or partially immersed in the gust. The wing's leading edge

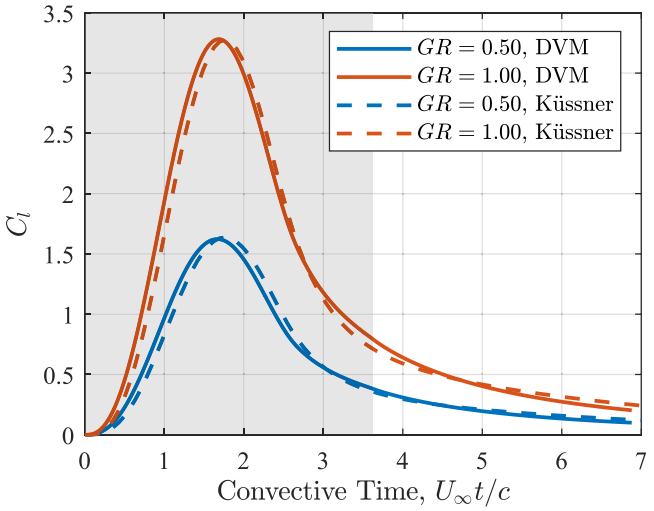

FIG. 3. The C_l response comparison of the wing encountering a sine-squared gust between the discrete vortex model with trailing-edge shedding and Küssner's gust response with a Duhamel integral at gust ratios 0.5 and 1.0.

enters the gust at $t^* = 0$. Figure 3 shows very close agreement between the discrete vortex model and Küssner's C_l response for gust ratios GR = 0.50 and 1.00, confirming that the discrete vortex model with the proposed gust representation and trailing-edge shedding yields results similar to existing theory.

Discrete vortex shedding at the leading edge is enforced in the following comparisons to capture the fully separated flow physics characteristic of large-amplitude transverse gust encounters. Figure 4 compares the vorticity field obtained from the discrete vortex model to the experimental vorticity field obtained from the University of Maryland's tow-tank facility using particle image velocimetry (PIV) at a Reynolds number Re = 20 000, gust-width-to-chord ratio $W/c = 2.62$, and GR = 1.00 [38]. The dashed lines indicate the nominal boundaries of the gust region. Note, however, that in experiments gust deformation due to wing-gust interactions can modify the gust's nominal region. The discrete vortex model accurately captures the evolution of the LEV and the overall flow field. The position and size of the LEV between the discrete vortex model simulation and the experimental PIV measurements agree. However, there is a noticeable difference in the angle of the leading-edge shear layer that can be seen at $t^* = 1.5$ and 2.0. The experimental PIV measurements show a more swept back shear layer. In addition, experimental data show significant leading-edge vorticity shedding at $t^* = 3.0$ when the leading edge is beyond the gust's nominal region, which the discrete vortex model does not capture. Uncertainty in the instantaneous gust

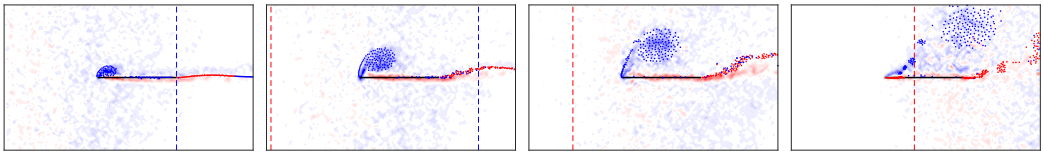

FIG. 4. Vorticity field comparison of a flat plate encountering a sine-squared gust acquired using PIV measurements [38] and the discrete vortex model at GR = 1.00 for various convective times t^*: (a) $t^* = 1.0$, (b) $t^* = 1.5$, (c) $t^* = 2.0$, and (d) $t^* = 3.0$.

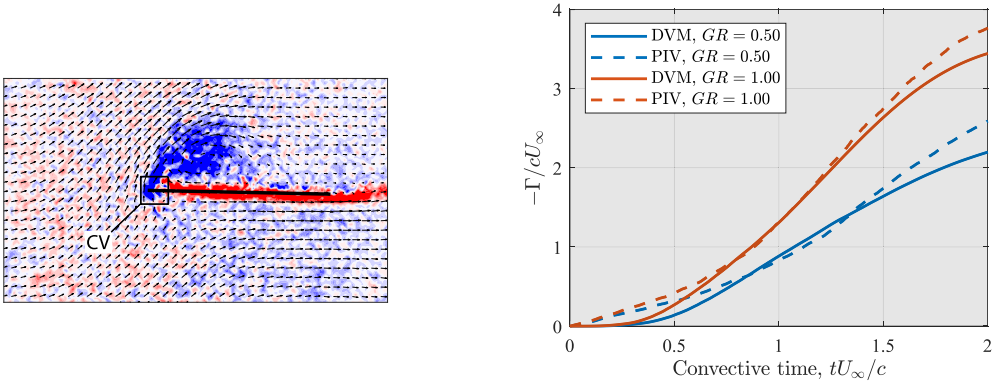

(a) (b)

FIG. 5. (a) Circulation production at the leading-edge comparison for the vortex model (DVM) and (b) the experimental measurements (PIV) [38] for gust ratios GR = 0.50 and 1.00.

location and deformation of the gust by the wing may offer possible explanations for the continued shedding of vorticity at the leading edge outside of the nominal gust region. The sine-squared profile of the gust is only a time-averaged approximation of the gust's velocity. In reality, the gust produced by the water tank gust generator meanders, and thus the instantaneous flow is not restricted to the nominal region. In addition, there are significant interactions between the wing and the gust during the encounter. The motion of the wing in the gust also deforms and spreads out the gust's shear layers [9,21,36] leading to nonzero gust velocity outside the gust's nominal bounds. Another possible reason for the continued shedding of circulation exhibited in experiments may be the induced effects of the shed vortex structures in the flow. Figure 4(d) shows that the shed leading-edge vorticity in experimental data is closer to the wing during the gust exit than in the DVM, resulting in stronger induced wake effects at the leading edge due to the wing's shed LEV and thus a higher vorticity shedding rate.

To validate the use of the Kutta condition at the leading edge in the discrete vortex model, the circulation of the initial LEV formation of the discrete vortex model is compared to experiments. Since the source of vorticity is difficult to determine in PIV images in the presence of gust vorticity, we do not measure the circulation of the LEV directly. Instead, to compute the LEV circulation from the experimental PIV measurements, a control volume (CV) is defined at the leading edge [as shown in Fig. 5(a)] and the circulation flux across the CV is computed according to the method outlined in Ref. [29]. Let s_l be a path on the perimeter of the CV. If all the vorticity produced at the leading edge feeds the LEV, then the rate of change of the LEV's circulation is equal to the vorticity flux crossing path s_l according to

$$\frac{d\Gamma}{dt} = \oint_{s_l} \omega \vec{u} \cdot \hat{n}\, ds_l, \tag{12}$$

where $\hat{n}$ is the unit vector normal to s_l.

Since the vorticity that feeds the LEV is negative, only the negative vorticity is used in calculating the rate of change of circulation of the LEV. Figure 5(a) shows that the CV used in the calculation is a square with a side length equal to 15% of the chord, centered offset from the leading edge so that it contains less of the gust's free vorticity. Figure 5(b) shows the history of the circulation of the LEV obtained from the vortex model and the PIV measurements for gust ratios GR = 0.50 and 1.00. Even though the time rate of change of the circulation, $d\Gamma/dt$, of the LEV is noisy due to the noise of the background gust, integrating that noisy signal in time according to Eq. (12) yields a Γ signal substantially smoother in Fig. 5(b). The circulation of the LEV in the vortex model agrees well with experiments for both gust ratios.

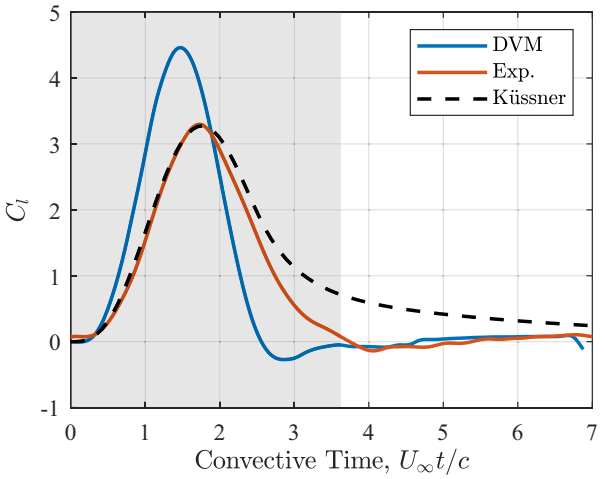

FIG. 6. The C_l time response obtained from the DVM, experimental measurements [38], and Küssner's model for GR = 1.00.

Figure 6 presents the lift coefficient results for the comparison of discrete vortex model simulations with leading- and trailing-edge shedding, experiments, and Küssner's analytical model. Even though the gust encounter experiments were carried out using a finite aspect ratio wing, the flow is fairly two dimensional for the majority of the encounter [39]. Since the wing is at $\alpha = 0^\circ$ prior to entering the gust in experiments, three-dimensional flow behavior, such as the development of tip vortices and trailed vorticity, starts building up once the wing enters the gust and does not have enough time to fully develop until the wing is exiting the gust. Thus, no aspect ratio correction is applied to the experimental lift measurements in this comparison.

The DVM captures the correct trend in lift, but overshoots Küssner's model and the experimental measurements. The formation of a strong LEV in the discrete vortex model leads to a C_l response higher than Küssner's attached flow gust response. Küssner's model and the experimental data force peaks agree, but the flow fields are significantly different. A substantial LEV is seen in the experimental data that is completely ignored in Küssner's inviscid model. Therefore, Küssner's model neglects a very important factor of the flow physics which may have an influence on the performance of the chosen closed-loop control method. The discrete vortex model yields a much better representation of the flow field despite its overprediction of lift. Previous works have introduced a circulation reduction factor to attenuate the forces predicted by the DVM and obtain better agreement with experiments [40]. These factors provide good force predictions at the expense of flow-field representation, and thus they were not used in this work. This suggests that there is physics in the experiments that is not captured by either the DVM or Küssner's inviscid model, but that ultimately results in an experimental force attenuation which yields closer agreement with Küssner's model. One example of this is that the DVM is inviscid and although it can be used to model separated flow, it does not capture viscous flow effects [41]. Viscous dissipation may act to dampen out the force peaks in the experimental data, leading to better agreement with the low force peak in the Küssner model. Specifically, the lack of viscous dissipation of the LEV in the DVM leads to an overprediction of lift. Even though Küssner's model is also inviscid, it does not model the LEV and thereby sidesteps the question of LEV viscous dissipation. The objective of this work is not only to regulate lift, but to also understand some of the flow mechanisms that are involved in regulating lift. Even though the DVM overpredicts the force, it captures important flow physics during a gust encounter. On the other hand, Küssner's model does not capture the vortex dynamics of fully separated flows, and thus provides an incomplete model for understanding flow-field contributions to the lift force. Since the DVM captures the correct vortical flow structures

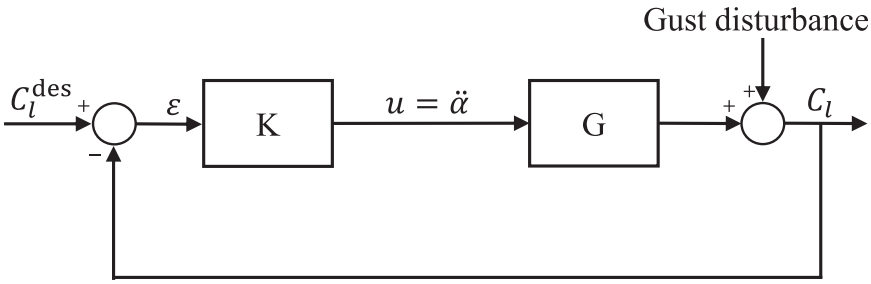

FIG. 7. Output feedback control framework.

and C_l general trend, it was chosen for use in simulating the flow field during the closed-loop control simulations of this paper.

III. LIFT REGULATION CONTROL DESIGN

This section presents a controller with the objective of regulating lift for a wing encountering a gust with an unknown strength and onset time. The gust is an unknown disturbance to be rejected by a controller that commands a pitch acceleration input. Linear robust control theory provides the tools necessary to develop the control law based on Theodorsen's linear lift response model. The performance of the linear robust controller is assessed by implementing it in simulation with the full nonlinear, discrete vortex model, in place of Theodorsen's model. This closed-loop control design is capable of mitigating the gust without prior knowledge of its strength or onset time.

Theodorsen's lift response model predicts the lift response of a wing for small amplitude, harmonic pitching, and plunging inputs. Nondimensionalizing by the semichord length b and the freestream velocity U_∞, the lift output is given in nondimensional form by [17]

$$C_l = \pi[\ddot{h} + \dot{\alpha} - a\ddot{\alpha}] + 2\pi\left[\alpha + \dot{h} + \dot{\alpha}\left(\tfrac{1}{2} - a\right)\right]C(k), \tag{13}$$

where $C(k)$ is a lift-deficiency function that models the impact of the wake on the circulatory contribution to lift, α is the geometric angle of attack, h is the plunge displacement, and a is the pitch axis position measured in semichords with respect to the midchord (e.g., pitching about the leading edge corresponds to $a = -1$, whereas the trailing edge is $a = 1$). Theodorsen's model [Eq. (13)] relies on the assumptions of attached flow, a planar and fixed wake, and small-amplitude motions. Even though these assumptions do not always hold, Theodorsen's model has been shown to adequately predict lift behavior outside its region of validity for a variety of different flows [42].

Brunton and Rowley [17] computed the transfer function of the C_l response to a pitch acceleration input $\ddot{\alpha}$ based on Theodorsen's model by taking the Laplace transform of Eq. (13),

$$G = \frac{\mathscr{L}\{C_l\}}{\mathscr{L}\{\ddot{\alpha}\}} = \pi\left[\frac{1}{s} - a\right] + 2\pi\left[\frac{1}{s^2} + \frac{1}{s}\left(\frac{1}{2} - a\right)\right]C(s) \tag{14}$$

where s is Laplace's variable nondimensionalized by U_∞/b. Using Jones's approximation of the lift-deficiency function [43], Eq. (14) can be expressed as

$$G(s) = \frac{4.7s^3 + 5.1s^2 + 1.85s + 0.086}{s^2(s^2 + 0.3455s + 0.01365)} \tag{15}$$

for a wing pitching about its midchord ($a = 0$).

Figure 7 shows the output feedback control framework used to design a controller that will regulate the lift of a wing about a desired value C_l^{des}. In this framework, the controller K computes the control input $u = \ddot{\alpha}$ based on the current value of the error $\varepsilon = C_l^{\text{des}} - C_l$. The calculated control input is applied to Theodorsen's unsteady aerodynamic model G given in Eq. (15), resulting in a C_l

output response. The gust is assumed to produce a linearly additive C_l disturbance. The current C_l measurement, based on the sum of Theodorsen's C_l response and the unknown gust disturbance, is fed back to the controller and the process repeats. When testing the controller, the plant G and the gust disturbance are replaced with the wing-gust encounter discrete vortex model. In the discrete vortex model, C_l can be readily computed due to full access to the flow field. In laboratory or real-world applications, C_l measurement may be possible using a force balance or by estimation using an array of pressure sensors distributed along the wing's chord.

The controller choice determines the frequency range of disturbances that the system can reject. Additive output disturbance rejection can be analyzed by calculation of the open-loop transfer function

$$L = GK \tag{16}$$

and the sensitivity transfer function

$$S = \frac{1}{1+L}. \tag{17}$$

The sensitivity transfer function should have low gains in frequency ranges where disturbances are expected to occur, thereby attenuating the influence of an additive output disturbance on the C_l output of the system. The nondimensional proportional control law

$$u = \ddot{\alpha} = k_p \varepsilon \tag{18}$$

results in the open-loop transfer function

$$L = \frac{4.7s^3 + 5.1s^2 + 1.85s + 0.086}{s^2(s^2 + 0.3455s + 0.013\,65)}\, k_p, \tag{19}$$

which yields the sensitivity transfer function

$$S = \frac{s^2(s^2 + 0.3455s + 0.013\,65)}{s^2(s^2 + 0.3455s + 0.013\,65) + (4.7s^3 + 5.1s^2 + 1.85s + 0.086)k_p}. \tag{20}$$

The nondimensional control gain k_p is selected based on rejection of disturbances by the sensitivity transfer function for disturbances within the applicable range of gust frequencies anticipated. For a gust with a sine-squared velocity profile of

$$v = V_{\max} \sin^2\left(\frac{U_\infty \pi}{W} t\right), \tag{21}$$

the reduced frequency is

$$k = \frac{\pi b}{W}. \tag{22}$$

For the simulations presented in Sec. IV, $b = 0.038$ m and $W = 0.2$ m, yielding $k = 0.60$. A nondimensional frequency is used to match the use of nondimensional variables in sensitivity transfer function (20). Figure 8 shows a Bode plot of the amplification $20\log_{10}(|S|)$ and the phase shift of the sensitivity transfer function for a range of reduced frequencies for the choice of $k_p = 1.05$ (corresponding to a dimensional feedback gain of 50). For the reduced frequency $k = 0.60$, this control law and choice of control gain yield $|S| = 0.084$, thereby attenuating output additive disturbances by approximately 91.6%.

Pitching the wing about the midchord is a special case where the $\ddot{\alpha}$ coefficient in Eq. (13) goes to 0. It was found that pitching the wing about points fore of the midchord ($a < 0$) provided similar gust rejection performance. Moving the pitching point aft of the midchord ($a > 0$) can lead to instability in the closed-loop system.

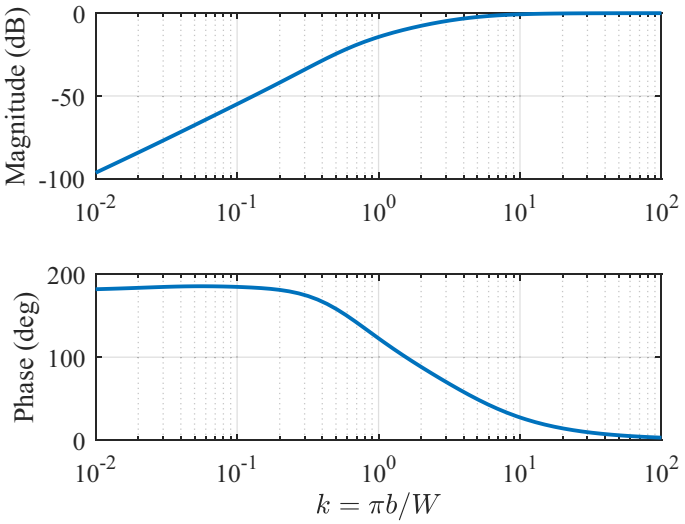

FIG. 8. Bode plot of the sensitivity transfer function S for $k_p = 1.05$.

IV. CLOSED-LOOP SIMULATIONS OF GUST ENCOUNTERS

This section demonstrates the ability of the proportional feedback control in regulating the lift force of a flat plate encountering a large-amplitude transverse gust. It also explains the different aerodynamic flow contributions during the gust encounter with and without closed-loop feedback control, underscoring the impact of closed-loop control on the flow physics of the gust encounter.

A. General C_l and pitch trends

The discrete vortex model of a flat plate at angle of attack $\alpha = 0^\circ$ encountering a gust with a sine-squared transverse velocity profile was run with and without closed-loop pitch control. Figures 9(a) and 10(a) show the C_l response with and without closed-loop control for gust encounters with gust ratios GR $= 0.50$ and 1.00, respectively. Figures 9(b) and 10(b) show the pitch kinematics for the actuated wing as calculated in the control loop. Figures 9(a) and 10(a) illustrate that introduction

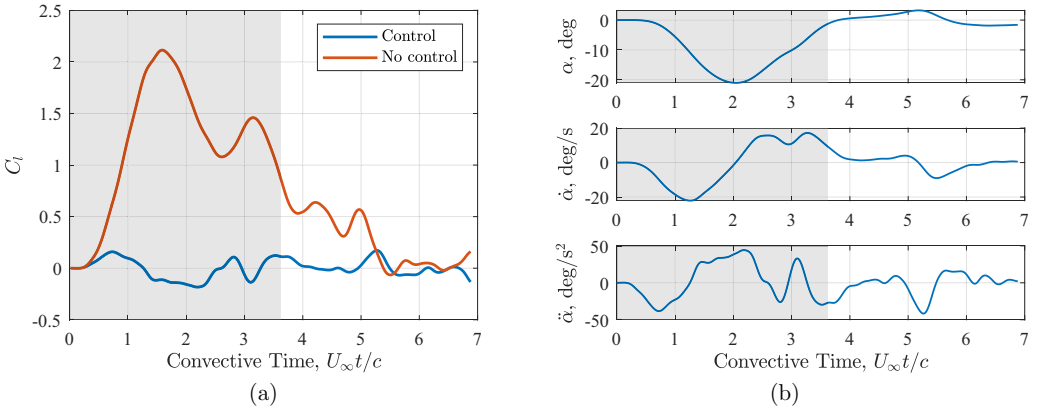

FIG. 9. (a) Coefficient of lift C_l response in a gust encounter with and without closed-loop control and (b) corresponding pitch kinematics for the wing with control for GR $= 0.50$.

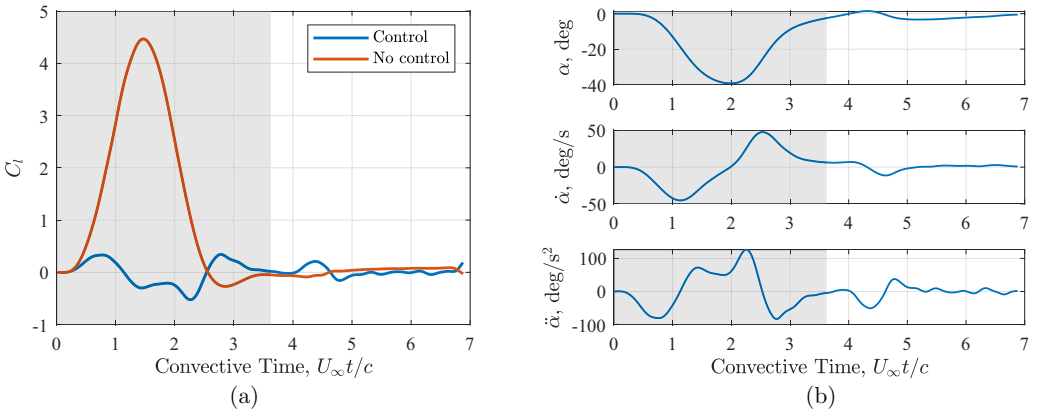

FIG. 10. (a) Coefficient of lift C_l response in a gust encounter with and without closed-loop control and (b) corresponding pitch kinematics for the wing with control for GR = 1.00.

of closed-loop proportional control can lead to a significant reduction in the C_l experienced by the wing. Closed-loop control reduced the peak C_l during the gust encounter by 92.3% for GR = 0.50 and by 91.8% for GR = 1.00. Figures 9(b) and 10(b) show that in both cases, the wing pitches down as it enters the gust and pitches up again as it exits the gust.

The results in Figs. 9 and 10 show that a proportional feedback control that was designed based on Theodorsen's linear unsteady aerodynamic model can regulate lift during a large-amplitude transverse gust encounter in spite of the significant violation of the model's assumptions of attached flow, a planar wake, and small pitching angles. For the gust in this scenario with a reduced frequency $k = 0.60$, the additive gust disturbance in a closed-loop system based on Theodorsen's linear model is theoretically attenuated by 91.60%, which is comparable to the reduction in the peak lift coefficients from the DVM simulations given the strong nonlinearity of the flow dynamics and the additional flow physics not captured by Theodorsen's linear inviscid model. The magnitudes of α, $\dot{\alpha}$, and $\ddot{\alpha}$ increase with gust ratio, suggesting that more aggressive pitching kinematics are needed to alleviate stronger gusts. Note that the pitching kinematics do not immediately go to zero beyond the gust region because the wing continues to experience transient aerodynamic effects beyond the gust due to its own wake (as shown at $t^* = 4$ in Figs. 11 and 12), causing pitch control to be

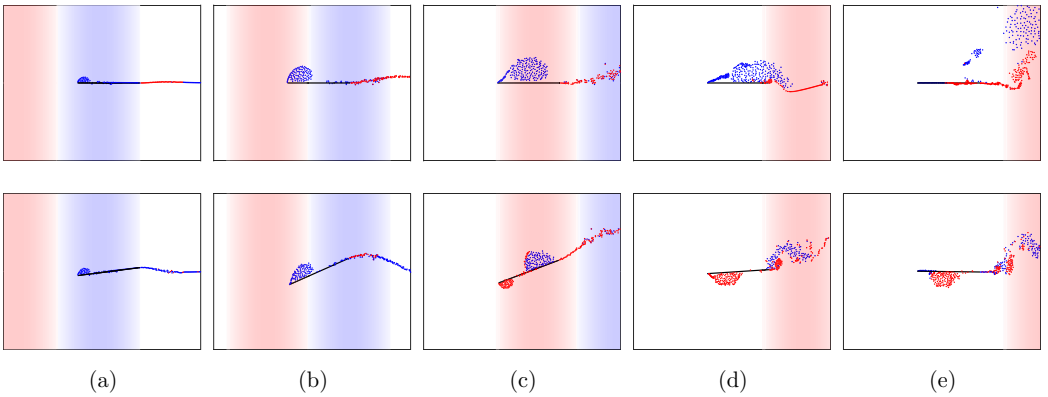

FIG. 11. Vorticity fields of a flat plate encountering a sine-squared gust at various convective times (a) $t^* = 1.00$, (b) $t^* = 1.65$, (c) $t^* = 2.60$, (d) $t^* = 3.50$, and (e) $t^* = 4.00$ for the case without control (top row) and the case with closed-loop pitch control (bottom row) at GR = 0.50.

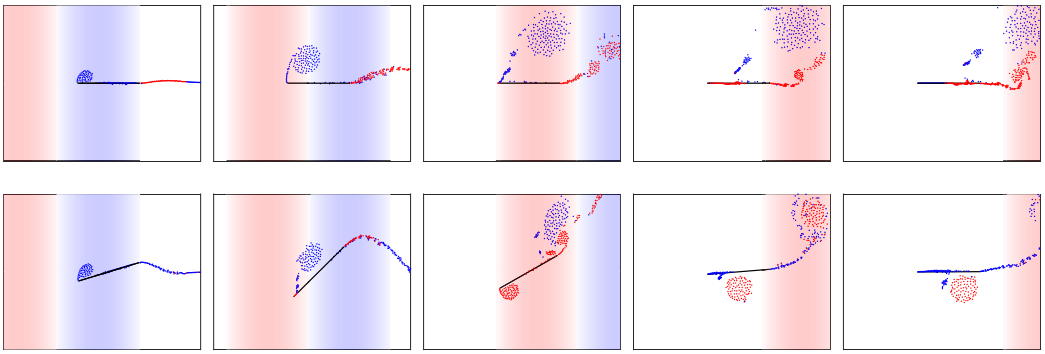

FIG. 12. Vorticity fields of a flat plate encountering a sine-square gust at various convective times (a) $t^* = 1.00$, (b) $t^* = 1.65$, (c) $t^* = 2.60$, (d) $t^* = 3.50$, and (e) $t^* = 4.00$ for the case without control (top row) and the case with closed-loop pitch control (bottom row) at GR $= 1.00$.

needed during the gust recovery region. The pitch rate magnitude for GR $= 1.00$ reaches 50 deg/s, which suggests that this closed-loop control strategy may be limited to vehicles that are capable of achieving such high pitch rates, such as small, agile, and unmanned vehicles. Open-loop control experiments performed in the University of Maryland tow tank and gust setup using a NACA0012 wing [15] have demonstrated force attenuation of the lift overshoot during a gust encounter using pitch rates that are comparable in magnitude to the rates achieved by the controller in this paper. This is evidence of the capability of the DVM at capturing the general trends of a pitch maneuver during a gust encounter.

B. Flow field and circulation trends

Figures 11 and 12 show the flow field during the gust encounter simulations with and without closed-loop control for a flat plate wing with angle of attack $\alpha = 0^\circ$ and gust ratios GR $= 0.50$ and 1.00, respectively. At GR $= 0.50$, as the wing enters the gust without control, it experiences a large flow upwash, creating a strong leading-edge shear layer which leads to the development of an LEV at $t^* = 1$ in Fig. 11. The shear layer continues to feed vorticity to the LEV and the vortex grows until approximately $t^* = 2.6$. As the wing reaches the latter half of the gust, the leading-edge shear layer feeding the LEV is disrupted. The LEV is shed and begins to convect away from the wing in the streamwise direction. At $t^* = 3.5$, a new leading-edge shear layer forms, injecting more vorticity into the flow as the wing exits the gust, corresponding to a secondary peak in the C_l response of Fig. 9(a) at approximately the same convective time. Throughout the gust encounter, the trailing-edge wake of the wing without control experiences an upwash from the gust, causing it to bend upward. At $t^* = 3.5$ in Fig. 11, the convecting LEV disrupts the trailing-edge shear layer and a new shear layer develops, forming a minor trailing-edge vortex (TEV).

For GR $= 1.00$, shown in Fig. 12, distinct differences in the flow field around the wing without control are apparent. A stronger LEV forms due to the stronger upwash experienced by the leading edge of the wing from the gust. In addition, the strong upwash of the gust causes the LEV to convect upward, detaching from the leading-edge shear layer at approximately the same convective time as in the GR $= 0.50$ gust encounter. The LEV convects upward as it sheds away from the wing and it induces the formation of a prominent TEV at $t^* = 3.5$ in Fig. 12.

The bottom rows of Figs. 11 and 12 show the impact of closed-loop control on the flow field of the gust encounter. Figure 11 at $t^* = 2.60$ and Fig. 12 at $t^* = 1.65$ and 2.60 show that the LEV detaches from the wing faster in the case of closed-loop control, which indicates that the shear layer is disrupted sooner. After the detachment of the LEV, a new opposite-signed LEV forms at

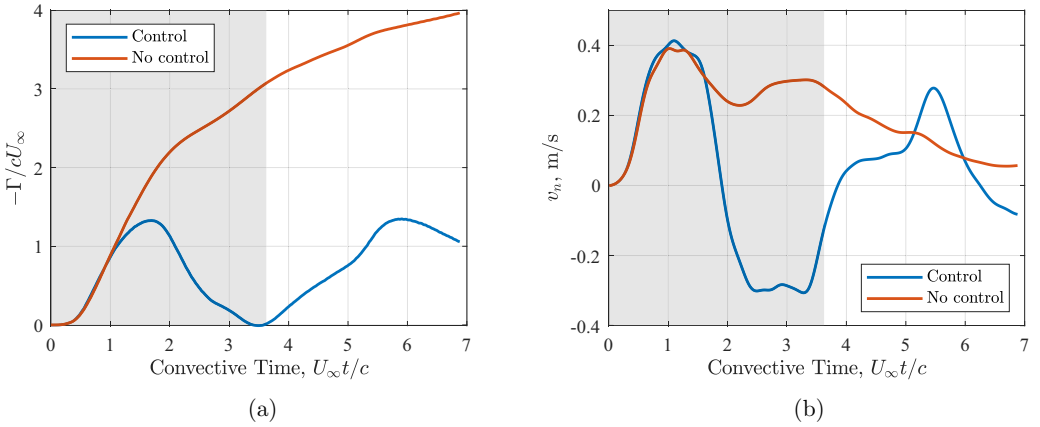

FIG. 13. (a) History of the total circulation produced by the leading edge and (b) history of the relative velocity normal to the leading edge of the wing for GR = 0.50.

$t^* = 2.60$. In the latter portion of the gust encounter, the wing's upward pitching motion and the greater freestream velocity component in the normal direction of the wing lead to a downwash experienced at the leading edge. The downwash at the leading edge creates the opposite-signed LEV. Similar to the gust encounter without control, the shed LEV induces the formation of a TEV. This TEV is more prominent in the case with GR = 1.00. The positive LEV lingers in the vicinity of the wing beyond the gust region ($t^* = 4.00$), leading to unsteady forces that require the pitch control to persist for a short duration beyond the gust.

Negative-signed clockwise vorticity that feeds the LEV is known to augment lift [44,45], so lift regulation may be achieved by a controller that acts to reduce the magnitude of circulation production from the leading edge throughout the encounter. Figures 13 and 14 show the evolution of the total circulation produced by the leading edge, along with the relative velocity normal to the leading edge of the wing. Figures 13(a) and 14(a) show that the closed-loop control is capable of regulating the total value of the circulation produced by the leading edge for both gust ratios, thereby mitigating the circulatory contribution to the force experienced by the wing, which is discussed further in Sec. IV C. Circulation production during the no-control scenario and during the

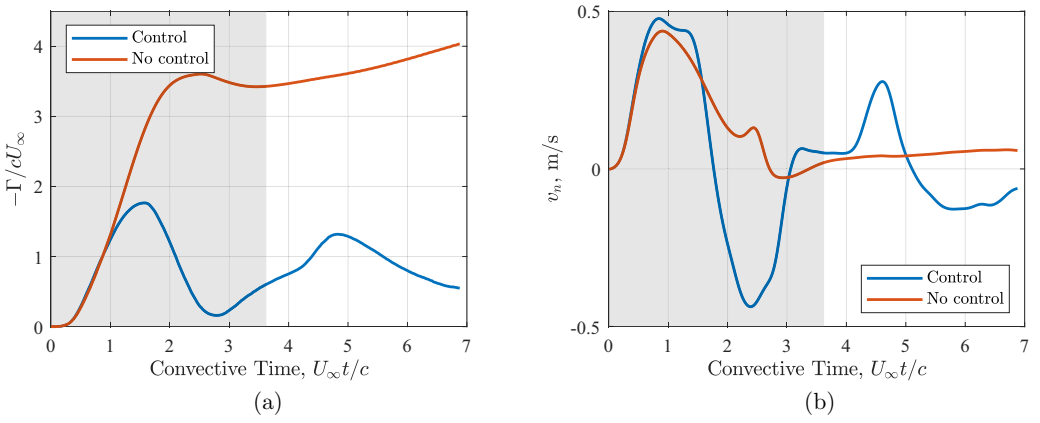

FIG. 14. (a) History of the total circulation produced by the leading edge and (b) history of the relative velocity normal to the leading edge of the wing for GR = 1.00.

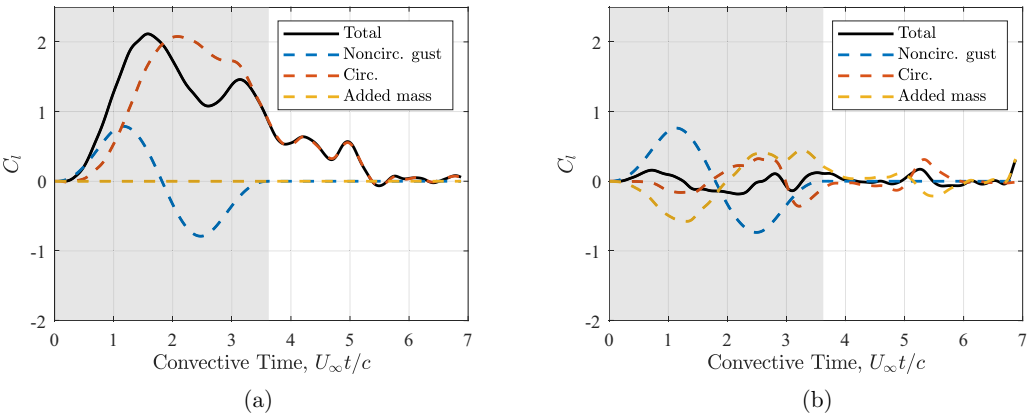

FIG. 15. Coefficient of lift C_l decomposition for the (a) no-control and (b) control cases at GR = 0.50.

closed-loop control scenario begin diverging at around $t^* = 1.65$, as shown in Figs. 13(a) and 14(a). At this point in the encounter, the wing's pitching leads to a reduction in the upwash experienced at the leading edge of the wing and then leads to a downwash, as shown in Figs. 13(b) and 14(b). First, reduced negative vorticity production occurs, followed by positive vorticity production, resulting in a reduction of the total circulation produced at the leading edge. As the wing exits the gust and pitches back up, the leading edge experiences an upwash again and the total negative circulation produced by the leading edge increases again.

An examination of these trends provides insight into the reasons a control law based on linear, classic unsteady aerodynamic theory is effective at regulating lift during a large-amplitude transverse gust encounter. The transverse velocity of the gust leads to an increase in the effective angle of attack experienced by the wing [46]. The direction of the initial pitch actuation that acts to reduce this increase is appropriately predicted by the setup in Fig. 7 with Theodorsen's model. The action of pitching the wing down as the wing enters the gust and pitching up as the wing exits the gust limits the increase of the effective angle of attack experienced by the wing throughout the encounter. Furthermore, closed-loop control leads to a decrease in circulation production from the leading edge and therefore reduces the influence of a strong LEV.

C. Contributions to C_l

In this section, Eq. (10) is used to decompose the lift that the wing experiences during an unsteady gust encounter into the noncirculatory gust force, the circulatory force, and the added-mass force. This decomposition is needed to understand the lift trends and to understand the aerodynamics associated with the controller's actions. Figures 15 and 16 show the decomposition of C_l into its individual contributions for the two gust ratios.

The decomposition presented in Figs. 15(a) and 16(a) shows that when no control is applied, most of the lift force comes from the circulatory contribution. The circulatory contribution overshadows the noncirculatory gust contribution and can be attributed to the formation of a strong leading-edge vortex during the gust encounter, as is evident in Figs. 13 and 14. The noncirculatory gust contribution rises as the wing enters the gust and the upwash from the gust increases with an increasing rate. As the wing approaches the center of the gust, the upwash continues increasing, but the rate of increase slows, leading the gust noncirculatory force contribution to decrease. Once the wing passes the center of the gust, the upwash experienced by the wing decreases, leading to a negative gust contribution just after $t^* = 2$, as shown in Figs. 15(a) and 16(a). As the wing exits the gust, the gust contribution returns to zero. The added-mass force is zero due to the absence of unsteady wing motion.

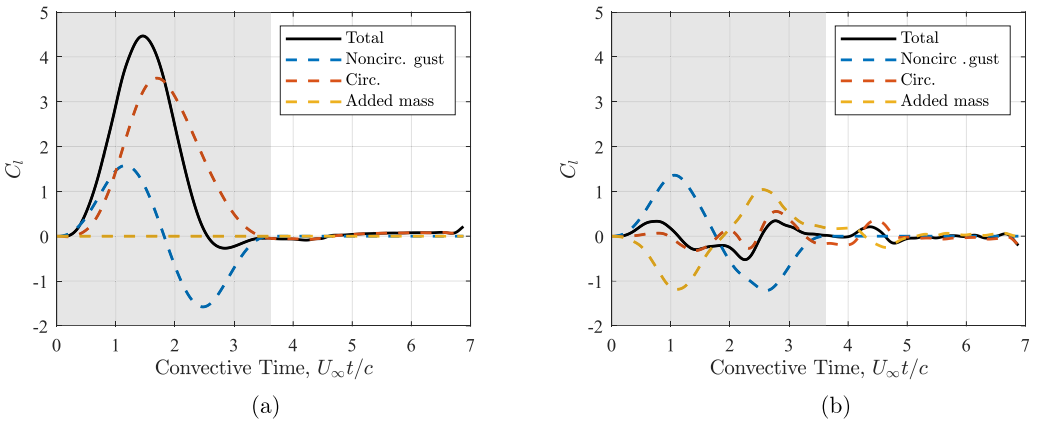

FIG. 16. Coefficient of lift C_l decomposition for the (a) no-control and (b) control cases at GR = 1.00.

Figures 15(b) and 16(b) reveal the aerodynamics involved in closed-loop gust mitigation. Closed-loop pitch control mitigates the circulatory contribution to the lift force by reducing the strength of the LEV and forming a second LEV with opposite-signed (positive) vorticity, as shown in Figs. 11 and 12, thereby reducing the total shed circulation from the leading edge. Closed-loop control leads to a slight reduction in the amplitude of the noncirculatory gust contribution. Variation in the noncirculatory gust contribution cannot be attributed to gust deformation, since it is not modeled in these simulations. The slight attenuation of the gust force is due to the variation of the component of the gust's velocity normal to the wing's chord. Even though the gust contribution is not mitigated, unlike the circulatory contribution, most of it is balanced by the added-mass contribution due to the pitching of the wing.

V. CONCLUSION

This paper provided a discrete vortex model for a flat plate encountering a transverse gust with a sine-squared velocity profile. The shedding behavior of the plate's edges was determined by enforcing the Kutta condition at both edges of the plate. The gust influenced the wing by imposing additional transverse velocity components based on the wing's position within the gust. Forces were evaluated using the vorticity impulse method derived by Wu [28], which relies on the rate of change of vorticity in the flow to obtain the forces. A useful decomposition of the vorticity in the flow was provided for a flat plate encountering a gust. This decomposition was used to deconstruct the lift contributions during the gust encounter with and without closed-loop control. The discrete vortex model with only trailing-edge shedding was validated using Küssner's gust response. The discrete vortex model with leading- and trailing-edge shedding was compared to experimental forces and PIV flow-field vorticity measurements obtained in the University of Maryland's tow-tank facility [38].

A simple proportional feedback control law for a pitch acceleration input was developed using tools from linear robust control. The control design was based on Theodorsen's linear lift response model. The control law and control gain were chosen to provide good disturbance rejection within an anticipated range of gust frequencies. The controller was tested in simulations with the full nonlinear, discrete vortex model for gust encounter scenarios with gust ratios GR = 0.50 and 1.00. The application of closed-loop control reduced the peak C_l during the gust encounter by 92.3% for GR = 0.50 and by 91.8% for GR = 1.00.

The flow fields of the gust encounters were studied to understand the efficacy of the closed-loop control. The application of closed-loop control led to a faster detachment of the LEV. After the detachment of the LEV, a new LEV of opposite sign (positive) formed. The wing's pitch motion and the freestream velocity component normal to the chord led to a downwash at the leading edge of the

wing, creating this positive LEV. Closed-loop control was shown to regulate the total circulation produced by the leading edge of the wing which mitigated the circulatory contribution to the lift force. The action of pitching the wing led to a reduction in the upwash experienced by the leading edge and then to a downwash leading to a reduction in the total circulation produced by the leading edge.

The total lift force was decomposed into its contributions to understand the mechanism by which closed-loop control was successful at regulating lift during the gust encounters. Without the application of closed-loop control, the circulatory contribution of the force was found to be higher than the noncirculatory gust contribution. This suggested that the strong lift peaks experienced during gust encounters were largely dominated by the vortex shedding behavior of the wing during the encounters. The noncirculatory contribution of the gust was positive as the wing entered the gust and became negative as the wing exited the gust. Closed-loop pitch control mitigated the circulatory contribution to the lift force by reducing the strength of the LEV and forming another LEV with an opposite-signed vorticity. The overall circulation produced by the leading edge was also significantly lower in the closed-loop control case. Closed-loop control led to only a slight reduction in the amplitude of the noncirculatory gust contribution to the C_l response. However, most of the gust contribution was balanced out by the added-mass contribution due to the pitching of the wing.

ACKNOWLEDGMENTS

The authors thank Ignacio Andreu, Pascal Gehlert, and Dr. Holger Babinsky for valuable discussions, as well as Hülya Biler for providing the experimental data shown in this work. The authors also gratefully acknowledge support from the Air Force Office of Scientific Research under Grant No. FA9550-16-1-0508 and the National Science Foundation under Grant No. 1553970.

[1] B. Moulin and M. Karpel, Gust loads alleviation using special control surfaces, J. Aircr. **44**, 17 (2007).

[2] D. J. Pines and F. Bohorquez, Challenges facing future micro-air-vehicle development, J. Aircr. **43**, 290 (2006).

[3] F. Boettcher, C. Renner, H.-P. Waldl, and J. Peinke, On the statistics of wind gusts, Bound.-Layer Meteorol. **108**, 163 (2003).

[4] O. Brasseur, Development and application of a physical approach to estimating wind gusts, Mon. Weather Rev. **129**, 5 (2001).

[5] S. Zarovy, M. Costello, A. Mehta, G. Gremillion, D. Miller, B. Ranganathan, J. S. Humbert, and P. Samuel, Experimental study of gust effects on micro air vehicles, in *AIAA Atmospheric Flight Mechanics Conference, Toronto, 2010* (AIAA, Reston, 2010), p. 7818.

[6] J. Taylor, Measurement of gust loads in aircraft, J. R. Aeronaut. Soc. **57**, 78 (1953).

[7] T. H. von Kármán and W. R. Sears, Airfoil theory for non-uniform motion, J. Aeronaut. Sci. **5**, 379 (1938).

[8] K. Viswanath and D. K. Tafti, Effect of frontal gusts on forward flapping flight, AIAA J. **48**, 2049 (2010).

[9] S. J. Corkery, H. Babinsky, and J. K. Harvey, On the development and early observations from a towing tank-based transverse wing–gust encounter test rig, Exp. Fluids **59**, 135 (2018).

[10] R. G. Cook, R. Palacios, and P. Goulart, Robust gust alleviation and stabilization of very flexible aircraft, AIAA J. **51**, 330 (2013).

[11] A. Oduyela and N. Slegers, Gust mitigation of micro air vehicles using passive articulated wings, Sci. World J. **2014**, 598523 (2014).

[12] M. Bhatia, M. Patil, C. Woolsey, B. Stanford, and P. Beran, Stabilization of flapping-wing micro-air vehicles in gust environments, J. Guid. Control Dyn. **37**, 592 (2014).

[13] H. Tebbiche and M. S. Boutoudj, Passive control on the NACA 4412 airfoil and effects on the lift, in *Design and Modeling of Mechanical Systems - II*, edited by M. Chouchane, T. Fakhfakh, H. Daly, N. Aifaoul, and F. Chaari, Lecture Notes in Mechanical Engineering (Springer, Cham, 2015), pp. 775–781.

[14] D. R. Williams and R. King, Alleviating unsteady aerodynamic loads with closed-loop flow control, AIAA J. **56**, 2194 (2018).
[15] G. Sedky, A. R. Jones, and F. D. Lagor, Lift regulation during transverse gust encounters using a modified Goman–Khrabrov model, AIAA J., 1 (2020) .
[16] T. Theodorsen, General theory of aerodynamic instability and the mechanism of flutter, NACA Report No. NACA-TR-496, 1949 (unpublished).
[17] S. L. Brunton and C. W. Rowley, Empirical state-space representations for Theodorsen's lift model, J. Fluid. Struct. **38**, 174 (2013).
[18] G. Perrotta and A. R. Jones, Unsteady forcing on a flat-plate wing in large transverse gusts, Exp. Fluids **58**, 101 (2017).
[19] C. Badrya and J. D. Baeder, Numerical study of a flat plate wing response to large transverse gusts at low Reynolds number, in *AIAA Scitech 2019 Forum, San Diego, 2019* (AIAA, Reston, 2019), paper 2019-0638.
[20] S. J. Corkery and H. Babinsky, An investigation into gust shear layer vorticity and the added mass force for a transverse wing-gust encounter, in *AIAA Scitech 2019 Forum, San Diego, 2019* (AIAA, Reston, 2019), paper 2019-1145.
[21] I. Andreu Angulo, H. Babinsky, H. Biler, G. Sedky, and A. R. Jones, Wing-gust interactions: The effect of transverse velocity profile, in *AIAA Scitech 2020 Forum, Orlando, 2020* (AIAA, Reston, 2020), paper 2020-0079.
[22] G.-H. Cottet and P. D. Koumoutsakos, *Vortex Methods: Theory and Practice* (Cambridge University Press, Cambridge, 2000), Vol. 8.
[23] J. Katz and A. Plotkin, *Low-Speed Aerodynamics* (Cambridge University Press, Cambridge, 2001), Vol. 13.
[24] K. Ramesh, A. Gopalarathnam, K. Granlund, M. V. Ol, and J. R. Edwards, Discrete-vortex method with novel shedding criterion for unsteady aerofoil flows with intermittent leading-edge vortex shedding, J. Fluid Mech. **751**, 500 (2014).
[25] D. Darakananda, A. F. d. C. da Silva, T. Colonius, and J. D. Eldredge, Data-assimilated low-order vortex modeling of separated flows, Phys. Rev. Fluids **3**, 124701 (2018).
[26] W. Hou, D. Darakananda, and J. D. Eldredge, Machine-learning-based detection of aerodynamic disturbances using surface pressure measurements, in *AIAA Scitech 2019 Forum, San Diego, 2019* (AIAA, Reston, 2019), paper 2019-1148.
[27] H. Chen and J. Jaworski, Aeroelastic encounters of spanwise vortex gusts and the self-rotation of trailing vortices, in *AIAA Scitech 2020 Forum, Orlando, 2020* (AIAA, Reston, 2020), paper 2020-0555.
[28] J. C. Wu, Theory for aerodynamic force and moment in viscous flows, AIAA J. **19**, 432 (1981).
[29] F. Manar and A. R. Jones, Evaluation of potential flow models for unsteady separated flow with respect to experimental data, Phys. Rev. Fluids **4**, 034702 (2019).
[30] X. Xia and K. Mohseni, Lift evaluation of a two-dimensional pitching flat plate, Phys. Fluids **25**, 091901 (2013).
[31] K. Ramesh, K. Granlund, M. V. Ol, A. Gopalarathnam, and J. R. Edwards, Leading-edge flow criticality as a governing factor in leading-edge vortex initiation in unsteady airfoil flows, Theor. Comput. Fluid Dyn. **32**, 109 (2018).
[32] M. Ol, G. Parker, G. Abate, and J. Evers, Flight controls and performance challenges for mavs in complex environments, in *AIAA Guidance, Navigation and Control Conference and Exhibit, Honolulu, 2008* (AIAA, Reston, 2008), paper 2008-6508.
[33] S. Watkins, J. Milbank, B. J. Loxton, and W. H. Melbourne, Atmospheric winds and their implications for microair vehicles, AIAA J. **44**, 2591 (2006).
[34] H. Biler, C. Badrya, and A. R. Jones, Experimental and computational investigation of transverse gust encounters, AIAA J. **57**, 4608 (2019).
[35] C. Wales, D. Jones, and A. Gaitonde, Prescribed velocity method for simulation of aerofoil gust responses, J. Aircr. **52**, 64 (2014).
[36] G. Sedky, F. Lagor, and A. R. Jones, The unsteady aerodynamics of a transverse wing-gust encounter with closed-loop pitch control, in *AIAA Scitech 2020 Forum, Orlando, 2020* (AIAA, Reston, 2020), paper 2020-1056.

[37] G. J. Leishman, *Principles of Helicopter Aerodynamics* (Cambridge University Press, Cambridge, 2006).
[38] H. Biler and A. R. Jones, Force prediction during transverse and vortex gust encounters, in *AIAA Scitech 2020 Forum, Orlando, 2020* (AIAA, Reston, 2020), paper 2020-0081.
[39] C. Badrya, J. D. Baeder, and A. R. Jones, Application of prescribed velocity methods to a large-amplitude flat-plate gust encounter, AIAA J. **57**, 3261 (2019).
[40] J. Katz, A discrete vortex method for the non-steady separated flow over an airfoil, J. Fluid Mech. **102**, 315 (1981).
[41] P. Hammer, A. Altman, and F. Eastep, Validation of a discrete vortex method for low Reynolds number unsteady flows, AIAA J. **52**, 643 (2014).
[42] M. V. Ol, L. Bernal, C.-K. Kang, and W. Shyy, Shallow and deep dynamic stall for flapping low Reynolds number airfoils, in *Animal Locomotion*, edited by G. K. Taylor, M. S. Triantafyllou, and C. Tropea (Springer, Cham, 2010), pp. 321–339.
[43] R. T. Jones, Operational treatment of the nonuniform-lift theory in airplane dynamics, NACA Report No. NACA-TN-667, 1938 (unpublished).
[44] C. P. Ford and H. Babinsky, Lift and the leading-edge vortex, J. Fluid Mech. **720**, 280 (2013).
[45] J. D. Eldredge and A. R. Jones, Leading-edge vortices: Mechanics and modeling, Annu. Rev. Fluid Mech. **51**, 75 (2019).
[46] G. Sedky, A. R. Jones, and F. Lagor, Lift modeling and regulation for a finite wing during transverse gust encounters, in *AIAA Scitech 2019 Forum, San Diego, 2019* (AIAA, Reston, 2019), paper 2019-1146.